

Evidence for Goldstone-like and Higgs-like structural modes in the model $\text{PbMg}_{1/3}\text{Nb}_{2/3}\text{O}_3$ relaxor ferroelectric

Sergey Prosandeev,¹ Sergei Prokhorenko,¹ Youstra Nahas,¹ A. Al-Barakaty,² L. Bellaiche,¹ Pascale Gemeiner,³ Dawei Wang,⁴ Alexei A. Bokov,⁵ Zuo-Guang Ye,⁵ and Brahim Dkhil³

¹Physics Department and Institute for Nanoscience and Engineering, University of Arkansas, Fayetteville, Arkansas 72701, USA

²Physics Department, Jamoum University College, Umm Al-Qura University, Makkah, Makkah 21955, Saudi Arabia

³Laboratoire Structures, Propriétés et Modélisation des Solides, CentraleSupélec, Université Paris-Saclay, CNRS-UMR8580, 91190 Gif-sur-Yvette, France

⁴School of Microelectronics & State Key Laboratory for Mechanical Behavior of Materials, Xi'an Jiaotong University, Xi'an 710049, China

⁵Department of Chemistry and 4D LABS, Simon Fraser University, 8888 University Drive, Burnaby, British Columbia, V5A 1S6, Canada



(Received 8 October 2019; revised 6 September 2020; accepted 9 September 2020; published 23 September 2020)

Effective Hamiltonian simulations are conducted to unveil the nature of the low-frequency polar modes in the prototype relaxor ferroelectric, $\text{Pb}(\text{Mg}_{1/3}\text{Nb}_{2/3})\text{O}_3$. Above the so-called T^* temperature, only a single soft-mode exists, with its frequency increasing under heating. On the other hand, for temperatures lower than the freezing temperature, this single soft-mode splits into two modes, with one mode slightly changing its low resonant frequency while the other exhibiting a resonant frequency sharply increasing under cooling, in agreement with previous measurements. More importantly, we present evidences that these two modes can be regarded as Goldstone-like and Higgs-like modes, inherent to the Mexican-hat-form of the atomic displacement potential we also reveal here, therefore extending the types of systems exhibiting Higgs-boson characteristics to relaxor ferroelectrics.

DOI: [10.1103/PhysRevB.102.104110](https://doi.org/10.1103/PhysRevB.102.104110)

I. INTRODUCTION

Because of their large dielectric constant, strong electrostriction, and giant piezoelectricity, relaxor ferroelectrics have attracted a lot of attention for more than 60 years [1–4]. However, their physics still remain an enigma of condensed matter. Puzzling phenomena were found in the prototypical relaxor ferroelectric, that is $\text{Pb}(\text{Mg}_{1/3}\text{Nb}_{2/3})\text{O}_3$ (PMN). For instance, at the Burns temperature of $T_d = 620$ K, the temperature dependence of birefringence, measured on cooling, deviates from a straight line [5,6], which was interpreted as the emergence of local finite polarization often coined as polar nanoregions, nanodomains, or nanoclusters. On further cooling, the dielectric permittivity does not obey the Curie-Weiss law [7] anymore and adopts a rounded peak at a finite and frequency-dependent temperature [1,2], while no macroscopic polarization appears down to 0K.

Moreover, unusual characteristics of *phonons* were found in neutron scattering measurements of PMN [8–11]. The authors of Ref. [9] observed a transverse optical (TO) phonon branch, altogether with the acoustic branch and central peak, emerging below T_d . According to the authors of Ref. [10], this phonon was strongly damped and its frequency decreased on cooling from 1100 K down to 600 K, then disappeared (which is called the waterfall phenomenon [10,12]) before reappearing below the freezing temperature of $\simeq 220$ K. Its frequency then increased when reducing the temperature below 220 K.

Several experiments reported that, in fact, the number of TO phonons having low frequency (less than 80 cm^{-1}) can be

more than one, which is surprising due to the overall cubic symmetry of PMN. For example, the authors of Ref. [11] discovered two optical modes denoted as TO1 (high-energy) and SM (low-energy), for temperatures above or close to T_d . A two-mode scenario was also found from the reflectivity spectra in PMN thin films [13] and bulks [14]. These two modes were named CM (low-frequency) and SM (high-frequency) in Ref. [13], versus $E_1(\text{TO1})$ and $A_1(\text{TO1})$ in Ref. [14]. This later notation suggests the possibility that the low-frequency mode corresponds to transverse fluctuations of local polarizations of polar nanoregions while the high-frequency mode is associated with longitudinal fluctuations of such local polarizations. Similarly, the authors of Ref. [15] found, via hyper Raman scattering that the lowest TO mode splits into two modes above T_d and down to about 500 K. The upper component well corresponds to the frequencies obtained in inelastic neutron scattering [10], while the low-frequency mode corresponds to the mode seen in the inelastic neutron spectra of Ref. [11] and in the far-infra-red spectra of Ref. [14]. Note that, in particular, combining data obtained from various spectroscopic measurements, the authors of Ref. [16] assumed that PMN responses can be interpreted as arising from randomly oriented anisotropic regions giving rise to two local dielectric functions, one along the axis parallel to their local dipole moments and the other perpendicular to it. This work and previous hyper-Raman measurements [17] even reported a third mode that is basically temperature independent, and was suggested to anticross with the single TO mode around T_d .

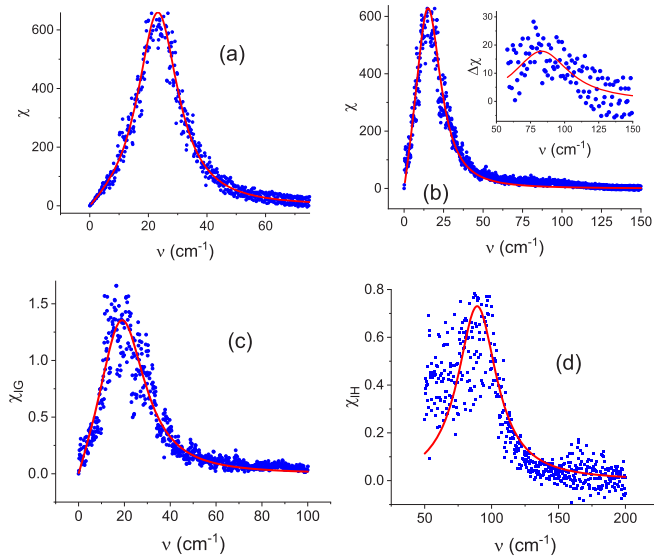


FIG. 1. Imaginary part of the dielectric response of PMN as a function of frequency at (a) 700 and (b) 50 K, along with the imaginary part of the (c) “local Goldstone” and (d) “local Higgs” responses at 50 K. The symbols show raw MD data, while the solid line displays the fit by one DHO. The inset in panel b represents the difference in the imaginary part between the raw dielectric response and its fit by one DHO at 50 K. Note that we do not show the interval below 50 cm^{-1} in the inset of panel (b) and in panel (d) to focus only on the numerically reliable high-frequency response.

Many questions therefore remain unanswered or controversial in PMN: how many low-frequency modes are there and for which temperature ranges? What is their temperature dependence? Can the third mode of Ref. [17] originate from chemical ordering, as proposed there? What are the microscopic origins of the other two low-frequency modes, and can these origins help in better understanding of the relaxor state? The goal of this article is to provide answers to all these questions by taking advantage of the idea of atomistic effective Hamiltonian [18] in general and of the atomistic effective Hamiltonian developed for PMN [19] in particular. As we will see, surprises are in store.

II. RESULTS

Let us now investigate dynamical properties of PMN, by performing molecular dynamics (MD) simulations using the numerical techniques described in the Supplemental Materials [20] and citation in the Supplemental Material [21]. Figures 1(a) and 1(b) report the imaginary part of the dielectric response as a function of the frequency for $T = 700 \text{ K}$ and 50 K , respectively. At both temperatures, these MD data are fitted reasonably well by a single damped harmonic oscillator (DHO) of the form $\chi_1(\nu) = \frac{\Omega_1^2}{\nu_1^2 - \nu^2 - i\Gamma_1\nu}$, where ν is the frequency, ν_1 is the resonant frequency (ν_1 is close to 25 cm^{-1} at 700 K versus 19 cm^{-1} at 50 K), Γ_1 is the damping constant, and Ω_1 is the plasma frequency. The inset of Fig. 1(b) also shows that, at 50 K , there is a small but noticeable peak of the dielectric response that is centered around a frequency of 86 cm^{-1} , to be denoted as ν_2 . To get the characteristics of

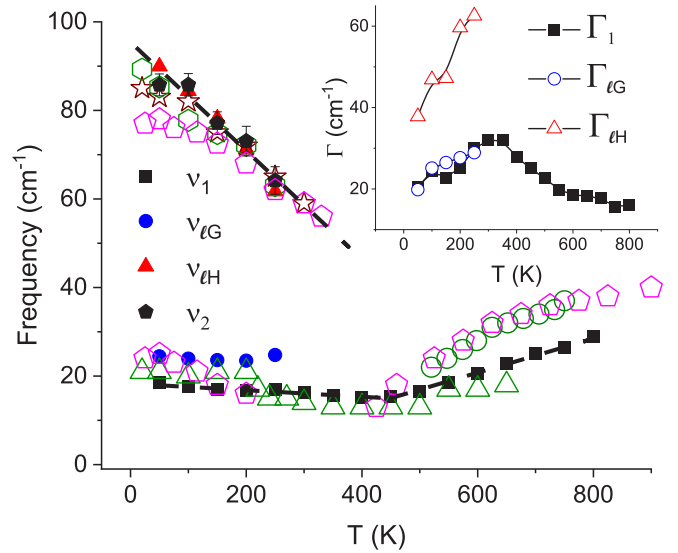


FIG. 2. Computed resonant frequencies in PMN as a function of temperature, as extracted from the total dielectric response. Experimental measurements are presented via the following open symbols: star [27], circle [15], pentagon [17], hexagon [10], and triangle [13]. The inset shows temperature dependence of the damping constants.

this weak peak, we first subtracted the DHO associated with ν_1 from the total dielectric response, and then fitted another DHO to the resulting difference.

Figure 2(a) reveals that ν_1 softens when the system is cooled down from 800 K to about 500 K (which is close to the characteristic T^* temperature of relaxor ferroelectrics [22,23]), similar to the behavior of the lowest-in-frequency (E_1) mode of Refs. [15,17,24] and of the single mode of Ref. [10]. Our predicted values of ν_1 above 500 K [25] are closer to the frequency of the central mode measured in thin films of PMN [13] than to the data of the low-frequency mode of Refs. [15,17]. Figure 2(a) further tells us that our ν_1 reaches its minimal values at around T^* before slightly increasing (from about 15 to 19 cm^{-1}) as the temperature decreases down to 10 K . These data are consistent with the temperature behavior of the central mode of Ref. [13] and with the mode denoted as $\omega_1/E(F_{1u})$ in Ref. [17]. The inset of Fig. 2 indicates that the Γ_1 damping parameter associated with ν_1 increases when cooling the system from high temperature to about T^* , as consistent with some measurements [6,15] for their lowest mode observed, before Γ_1 more-or-less saturates for temperatures varying between 250 and 400 K . Below 250 K , Γ_1 then starts to slightly decrease with temperature, which is also in-line with experiments [26]. Measured amplitudes of the damping constant for the lowest mode (e.g., 23 cm^{-1} at 300 K in Ref. [6] and 38 cm^{-1} at 300 K in Ref. [26]) are of the same order than our predictions for Γ_1 .

Regarding our higher-in-frequency mode, its ν_2 resonant frequency adopts the temperature behavior of the “soft mode” in Refs. [10,27] and of the mode coined as $\omega_3/A_1(F_{1u})$ in Ref. [17], namely a significant decrease when the temperature increases from small values to about 250 K (in fact, the square of the ν_1 and ν_2 frequencies is nearly linearly dependent on temperature both below and above 450 K). Our computed

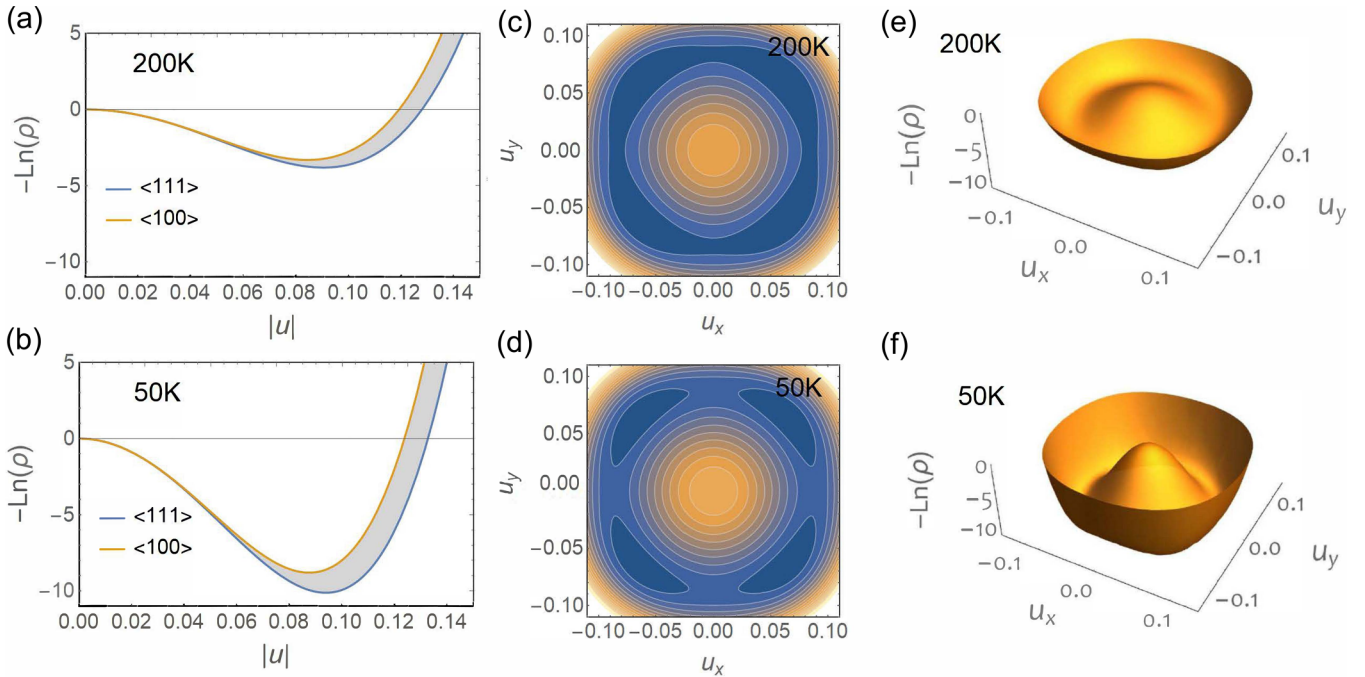


FIG. 3. Data related to potential for the temperature of 200 and 50 K. (a), (b) Dependence of $-\text{Ln} \rho(u_x, u_y, u_z)$ on the amplitude of the local mode $|u|$ plotted along different crystallographic directions. The blue and yellow curves correspond to the local mode vectors being oriented along the pseudocubic $\langle 111 \rangle$ and $\langle 100 \rangle$ directions, respectively. Curves corresponding to other orientations of this local mode vector fill the shaded area. (c), (d) Isopotential lines of the effective potential in a (001) plane; and (e), (f) Effective potential $-\text{Ln} \rho(u_x, u_y, 0)$ as a function of the x and y components of the local modes. Note that we use in panels (c) and (d) orange and navy colors for marking the maximum and minimum of the potential correspondingly.

values of ν_2 below 250 K also agree rather well with the measured data of Refs. [10,17,27]. We did not report the damping constant and plasma frequency of the high-frequency mode in Figs. 2(b) and 2(c) because they are difficult to accurately obtain, given the weak intensity of this mode. All these good agreements between our predictions and measurements provide a further support to our adopted model of damped harmonic oscillators to fit our calculated total dielectric response. Note also, that unlike for the choice of damped harmonic oscillators, using a Debye response for the low-in-frequency mode did not provide a good fit of our MD data.

Note also that, similar to the experimental work of Ref. [17], we tried to fit our data using a third DHO between 25 and 200 K. This fit was not reliable, mostly due to a strong overlap with our low-in-frequency ν_1 mode. In other words, we did not find any obvious evidence that a third zone-center mode should exist in our data. This likely implies that the third mode of Ref. [17] is either associated with the existence of chemically ordered regions inside PMN (while we mimic a chemically disordered system) or that such mode corresponds to an off-center k -point (as additional calculations we performed suggest, see the Supplemental Materials [20]).

Let us now reveal the microscopic origin of our two modes. For that, we first evaluate, from Monte Carlo simulations, the probability, ρ , for lead-centered dipoles to have a certain amplitude along different crystallographic directions [28]: ρ is a single-variable distribution function, which corresponds to a three-dimensional normalized histogram of the values of the local mode vectors (that are directly proportional to local dipoles) at the Pb sites of the supercell and that is

calculated over 2×10^6 sweeps after prior thermalization over 10^5 sweeps. The local effective potential is then estimated via $V_{\text{eff}} = -k_B T \text{Ln}(\rho/A)$, where A is a normalizing coefficient. In Figs. 3(a) and 3(b), we show the dimensionless local effective potential $-\text{Ln} \rho(u_x, u_y, u_z)$ (i.e., V_{eff} in units of $k_B T$, and where u_x, u_y, u_z are the Cartesian components of the local mode) as a function of the amplitude of the local modes for different crystallographic directions, at 200 and 50 K, respectively. In Figs. 3(c) and 3(d), we show the isopotential lines of this effective potential in a (001) plane at these two temperatures, while Figs. 3(e) and 3(f) display the corresponding $-\text{Ln} \rho(u_x, u_y, 0)$ as a function of the x and y components of the local mode. Figures 3(a) to 3(d) demonstrate that the potential is rather isotropic for dipolar amplitude smaller than about 0.05 (in arbitrary units). They also show that this potential becomes slightly anisotropic for larger dipolar amplitude with narrow wells that deepen with decreasing temperature, which also results in a larger anisotropy when temperature is reduced. The values of the dipolar amplitude associated with the minima of the wells, for different crystallographic directions, is rather insensitive to the change in temperature from 200 to 50 K unlike the energy of these wells, which is consistent with the idea of a dipolar freezing setting in below 210 K in PMN [3]. Note also that (i) our finding that the $\langle 111 \rangle$ directions correspond to the minimum in energy for both 200 and 50 K is in-line with Refs. [29,30] indicating that the displacement of Pb atoms exhibit preference along $\langle 111 \rangle$ directions below 300 K; and (ii) our local potential displayed in Fig. 3(c) is similar to the density distribution around Pb ions recently extracted from

x-ray powder diffraction measurements and Rietveld analysis in Ref. [30] for PMN at 300 K and from neutron scattering analysis at 293 K in Ref. [31].

The aforementioned features of Figs. 3(a) to 3(d) result in the effective potential acquiring a “Mexican hat” shape, as seen in Figs. 3(e) and 3(f), with the decrease in temperature having two noticeable effects: (1) the “center of the hat” (which is an energy barrier) is higher with respect to the lowest energies of the hat because of the deepening of the wells; and (2) the “brim of the hat” becomes more distorted because of a more pronounced anisotropy. Figures 3(e) and 3(f) motivate us to check if the modes having the ν_1 and ν_2 resonant frequencies can be related to the so-called Goldstone-like and Higgs-like modes since these later modes are linked to the existence of a potential having a Mexican hat shape or $U(1)$ symmetry [32–37]. So far, these properties have not been discovered in ferroelectric relaxors, to the best of our knowledge. If so, relaxor ferroelectrics will join the family of condensed matter systems with outstanding properties such as superfluids, superconductors, uniaxial antiferromagnets, or charge-density waves [38]. Those systems show broken continuous symmetry phenomenon whose nature shares close similarities with the so-called Higgs boson in particle physics.

To investigate such possibility, we selected regions around each Pb site i of the supercell that contain this site i as well as its six nearest Pb neighbors, 12 second nearest Pb neighbors and eight third nearest Pb neighbors. For any selected temperature below 250 K, the dipole moment \mathbf{p}_i , as averaged over these 27 sites and the first 10^5 MD steps, was computed for each region centered around each site i in our $18 \times 18 \times 18$ supercell. The direction of this dipole moment is now our new local z'_i axis. Two other new local axes, x'_i and y'_i , were defined to lie transverse to z'_i : one vector was along $(-p_{iy}, p_{ix}, 0)$ and the other was orthogonal to this vector and to \mathbf{p}_i . For any time beyond the first 10^5 MD steps, we calculated the local dipole moment \mathbf{d}_i as an average over the 27 sites for each miniregion in our supercell, then projected these dipole moments onto the local x'_i , y'_i , and z'_i directions, averaged over the site i , and inserted the result in place of $d(t)$ in Eq. (1) of the Supplemental Materials [20]. This results in the generation of a novel $x'x'$, $y'y'$, and $z'z'$ types of local dielectric responses. The $x'x'$ and $y'y'$ responses were found to be similar and are coined here as the “local Goldstone” response since they correspond to the fluctuations being *transverse* to the local polarization.

To search for the origin of the highest-frequency mode, we tried two options. (1) The first one is to replace $d(t)$ of Eq. (1) of the Supplemental Materials [20] by the z'_i -component of the dipole moment (then averaged over the local z'_i directions), which corresponds to the computation of a local A-TO mode. (2) The second one is to use, for $d(t)$ of Eq. (1) of the Supplemental Material [20], the averaged over the sites i dipole’s *amplitude* associated with the 27-site region centered around site i . Such second way corresponds to the computation of the Higgs mode since it is associated with the fluctuations of the *scalar amplitude* of the dipoles, as similar to the concept of the Higgs mode. As demonstrated in the Supplemental Material [20], these two options give similar results, and the resulting response is termed here the “local Higgs” response. Note that the experimental

search of Higgs-like mode is difficult in PMN as the global macroscopic symmetry is not broken and, correspondingly, it does not couple linearly to the usual condensed matter probes [33], as illustrated by the weak and overdamped response in our dielectric data [see inset of Fig. 1(b)].

The imaginary part of the “local Goldstone” and “local Higgs” responses is shown in Figs. 1(c) and 1(d), respectively, at 50 K. The local Goldstone-like response adopts a peak that can be well fitted by a single DHO with a resonant frequency to be denoted as ν_{IG} and that is close to 25 cm^{-1} for a temperature of 50 K. Such ν_{IG} frequency is therefore rather close to the ν_1 frequency obtained from the total dielectric response at 50 K and equal to 19 cm^{-1} . Figure 1(d) reveals a broad peak for the “local Higgs” responses that can also be well fitted by a single DHO, with a resonant frequency to be called as ν_{IH} and that is equal to 90 cm^{-1} at 50 K. Such value is remarkably close to the ν_2 frequency for the same temperature of 50 K, which is extracted from the total dielectric response. As further reported in Fig. 2(a), we were able to extract ν_{IG} and ν_{IH} for any temperature up to 350 K. The inset in Fig. 2 reports the damping parameter of these “local Goldstone” and “local Higgs” responses, to be denoted by Γ_{IG} and Γ_{IH} , respectively. It is clear from Fig. 2 that the ν_{IG} and ν_1 frequencies are very close to each other for any temperature studied, which attests that the lowest frequency of the total dielectric response is associated with the Goldstone-like mode. Such conclusion is reinforced by the damping parameter associated with ν_{IG} being close to Γ_1 for any temperature studied, as revealed by the inset in Fig. 2. Similarly, Fig. 2 shows the close proximity of ν_{IH} and ν_2 , for any temperature studied. In other words, the higher frequency of the total dielectric response can be asserted to correspond to a Higgs-like mode.

Note that PMN does not have any macroscopic polarization down to 0 K. Consequently, the macroscopic symmetry is not broken. What happens in this relaxor ferroelectric is that, below some temperature, some relatively small regions can exhibit a polarization having a static or quasistatic character, but with the direction of this local polarization changing from one region to another (such as to conserve a total vanishing polarization). For each of these regions, one mode corresponds to the vibration being transverse to the polarization of the region (which can be thought as being a local E-TO mode vibration) while the other mode is associated with the vibration along the polarization of that region (which can be thought as being a local A-TO mode). Since the direction of local polarization changes in space, we rather decided to use the correlators we designed to demonstrate that the first mode can in fact be associated with the (local) Goldstone-like mode while the second mode is related to the (local) Higgs-like mode, but in Riemannian-type coordinate system, which depends on the point in space of the crystal. Moreover, the fact that we numerically found a Mexican hat form for the atomic displacement potential is also consistent with this idea of the Goldstone- and Higgs-like boson modes in PMN we found. This kind of atomic displacement potential does also exist up to 650 K as shown in the Supplemental Material (in addition to our own experiments that confirm the accuracy of our calculations) [20]. These two modes can be extracted from the aforementioned special and new correlators only if we well determine the direction of the local polarization. We found

that this is technically feasible only below 350 K because the dipolar dynamics is rather intense above this temperature. This can either mean that the ν_{IG} and ν_{IH} modes exist only below 350 K or, more likely, that it is numerically difficult to extract them above 350 K. The first case corresponds to a first-order transition at 350 K while the second possibility is associated with a phase transition at 450 K (T^*) or even at 620 K (Burns' temperature). Note also that the insets of Fig. 2 do show that the Γ constants are rather large near 350 K, therefore demonstrating the overdamped nature of the modes and thus explaining the difficulty in obtaining them above 350 K. We adopted a model of damped harmonic oscillators to fit them to the total dielectric response simply because it fits very well. Those are in very good agreement with experimental data, as shown in Fig. 2(a). This also confirms the validity of our approach. We also numerically found that using a Debye response for the low-in-frequency mode does not provide a good fit of the MD data.

III. CONCLUSION

In conclusion, on the basis of first-principles-based effective Hamiltonian molecular dynamics simulations conducted on disordered PMN, our main results are that (1) only a single low-frequency polar mode is found above T^* with its resonance frequency decreasing on cooling (note that further simulations indicated in the Supplemental Materials [20] suggest that the additional mode reported in Ref. [17] is associated with an off-center k -point); (2) two polar modes

then emerge with rather different temperature behaviors: the lowest-in-frequency mode has a resonant frequency that only slightly changes with temperature while the highest-in-frequency mode adopts a strongly temperature-dependent resonant frequency; and (3) these two later modes can be thought as resulting from the occurrence of a Mexican-hat-shape local effective potential in PMN (that we also report here) and can be assigned to be Goldstone-like and Higgs-like modes. We hope that the present discoveries deepen the current understanding of relaxor ferroelectrics, as well as, further link Higgs-boson-like physics and condensed matter. In particular, it is important to realize that we evidenced Higgs-boson-like modes near room temperature in PMN, while other previously reported systems (superconductors, antiferromagnets, charge density waves, or cold atoms) exhibit Higgs-like-mode-driven properties at rather low temperatures [38].

ACKNOWLEDGMENTS

This work is financially supported by the ONR Grant No. N00014-17-1-2818 (Sergey P. and L.B.), the Vannevar Bush Faculty Fellowship (VBFF) Grant No. N00014-20-1-2834 from the Department of Defense (Sergei P. and L.B.), the DARPA Grant No. HR0011727183-D18AP00010 (TEE Program) (Y.N. and L.B.), the ONR Grant No. N00014-16-1-3106 (A.A.B. and Z.G.Y.), the Natural Sciences and Engineering Research Council of Canada (NSERC) Discovery Grant No. RGPIN-2017-06915 (Z.G.Y.), and the NSFC Grant No. 11974268 (D.W.).

-
- [1] G. A. Smolensky and A. I. Agranovskaya, *Sov. Phys. Tech. Phys.* **3**, 1380 (1958).
 - [2] L. E. Cross, *Ferroelectrics* **151**, 305 (1994).
 - [3] D. Viehland, S. J. Jang, L. E. Cross, and M. Wuttig, *Philos. Mag. B* **64**, 335 (1991).
 - [4] E. V. Colla, E. Yu. Koroleva, N. M. Okuneva, and S. B. Vakhrushev, *Ferroelectrics* **184**, 209 (1996).
 - [5] G. Burns and F. H. Dacol, *Phys. Rev. B* **28**, 2527 (1983); *Sol. St. Commun.* **48**, 853 (1983).
 - [6] O. Svitelskiy, J. Toulouse, G. Yong, and Z.-G. Ye, *Phys. Rev. B* **68**, 104107 (2003).
 - [7] F. Jona and G. Shirane, *Ferroelectric Crystals* (Pergamon, Oxford, 1962).
 - [8] C. Stock, L. Van Eijck, P. Fouquet, M. Maccarini, P. M. Gehring, G. Xu, H. Luo, X. Zhao, J.-F. Li, and D. Viehland, *Phys. Rev. B* **81**, 144127 (2010).
 - [9] A. Naberezhnov, S. Vakhrushev, B. Dorner, D. Strauch, and H. Moudén, *Eur. Phys. J. B* **11**, 13 (1999).
 - [10] S. Wakimoto, C. Stock, R. J. Birgeneau, Z.-G. Ye, W. Chen, W. J. L. Buyers, P. M. Gehring, and G. Shirane, *Phys. Rev. B* **65**, 172105 (2002).
 - [11] S. B. Vakhrushev and S. M. Shapiro, *Phys. Rev. B* **66**, 214101 (2002); S. B. Vakhrushev, R. G. Burkovsky, S. Shapiro, and A. Ivanov, *Phys. Sol. Stat.* **52**, 889 (2010).
 - [12] J. Hlinka, S. Kamba, J. Petzelt, J. Kulda, C. A. Randall, and S. J. Zhang, *Phys. Rev. Lett.* **91**, 107602 (2003).
 - [13] S. Kamba, M. Kempa, V. Bovtun, J. Petzelt, K. Brinkmann, and N. Setter, *J. Phys. Condens. Matter* **17**, 3965 (2005).
 - [14] J. Hlinka, T. Ostapchuk, D. Noujni, S. Kamba, and J. Petzelt, *Phys. Rev. Lett.* **96**, 027601 (2006).
 - [15] A. Al-Zein, J. Hlinka, J. Rouquette, and B. Hehlen, *Phys. Rev. Lett.* **105**, 017601 (2010).
 - [16] D. Nuzhnyy, J. Petzelt, V. Bovtun, M. Kempa, S. Kamba, J. Hlinka, and B. Hehlen, *Phys. Rev. B* **96**, 174113 (2017).
 - [17] B. Hehlen, M. Al-Sabbagh, A. Al-Zein, and J. Hlinka, *Phys. Rev. Lett.* **117**, 155501 (2016).
 - [18] W. Zhong, D. Vanderbilt, and K. M. Rabe, *Phys. Rev. B* **52**, 6301 (1995).
 - [19] A. Al-Barakaty, S. Prosandeev, D. Wang, B. Dkhil, and L. Bellaiche, *Phys. Rev. B* **91**, 214117 (2015).
 - [20] See Supplemental Materials at <http://link.aps.org/supplemental/10.1103/PhysRevB.102.104110> for additional details of our calculations.
 - [21] I. Ponomareva, L. Bellaiche, T. Ostapchuk, J. Hlinka, and J. Petzelt, *Phys. Rev. B* **77**, 012102 (2008).
 - [22] H. Takenaka, I. Grinberg, and A. M. Rappe, *Phys. Rev. Lett.* **110**, 147602 (2013); I. Grinberg and A. M. Rappe, *Phys. Rev. B* **70**, 220101(R) (2004).
 - [23] B. Dkhil, P. Gemeiner, A. Al-Barakaty, L. Bellaiche, E. Dulkan, E. Mojaev, and M. Roth, *Phys. Rev. B* **80**, 064103 (2009).
 - [24] M. Al Majzoub Al Sabbagh, Ph.D. thesis, Université de Montpellier, 2016.
 - [25] Note, however, that using a mass being 2.25 smaller than the one we employ here will make our ν_1 agreeing rather well with the data of Refs. [26, 10, 15, 17] above 400 K.

- [26] H. Taniguchi, M. Itoh, and D. Fu, *J. Raman Spectrosc.* **42**, 706 (2011); D. Fu, H. Taniguchi, M. Itoh, S.-Y. Koshihara, N. Yamamoto, and S. Mori, *Phys. Rev. Lett.* **103**, 207601 (2009).
- [27] V. Bovtun, S. Kamba, A. Pashkin, M. Savinov, P. Samoukhina, J. Petzelt, I. P. Bykov, and M. D. Glinchuk, *Ferroelectrics* **298**, 23 (2004).
- [28] J.-M. Kiat, G. Baldinozzi, M. Dunlop, C. M. B. Dkhil, C. Ménoret, O. Masson, and M.-T. Fernandez-Diaz, *J. Phys.: Condens. Matter* **12**, 8411 (2000).
- [29] M. Eremenko, V. Krayzman, A. Bosak, H. Y. Playford, K. W. Chapman, J. C. Woicik, B. Ravel, and I. Levin, *Nat. Commun.* **10**, 2728 (2019).
- [30] S. Noda, Y. Yokoi, Y. Nakahira, T. Abe, I. Fujii, T. Wada, C. Moriyoshi, and Y. Kuroiwa, *Jpn. J. Appl. Phys.* **58**, SLLA06 (2019).
- [31] S. B. Vakhrushev and N. M. Okuneva, in *Fundamental Physics of Ferroelectrics 2002*, edited by R. E. Cohen, AIP Proc. Conf. no. 626 (Melville, NY, 2002).
- [32] M. Endres, T. Fukuhara, D. Pekker, M. Cheneau, P. Schaub, C. Gross, E. Demler, S. Kuhr, and I. Bloch, *Nature* **487**, 454 (2012).
- [33] D. Podolsky, A. Auerbach, and D. P. Arovas, *Phys. Rev. B* **84**, 174522 (2011).
- [34] S. Lin *et al.*, *Nat. Phys.* **10**, 970 (2014).
- [35] S. M. Nakhmanson and I. Naumov, *Phys. Rev. Lett.* **104**, 097601 (2010).
- [36] A. Marthinsen, S. M. Griffin, M. Moreau, T. Grande, T. Tybell, and S. M. Selbach, *Phys. Rev. Materials* **2**, 014404 (2018).
- [37] A. D. Bruce and R. A. Cowley, *J. Phys. Solid State* **11**, 3609 (1978).
- [38] D. Pekker and C. M. Varma, *Annu. Rev. Condens. Matter Phys.* **6**, 269 (2015).